

PlanScope: Learning to Plan Within Decision Scope for Urban Autonomous Driving

Ren Xin, Jie Cheng, Hongji Liu, and Jun Ma, *Senior Member, IEEE*

Abstract—In the context of urban autonomous driving, imitation learning-based methods have shown remarkable effectiveness, with a typical practice to minimize the discrepancy between expert driving logs and predictive decision sequences. As expert driving logs natively contain future short-term decisions with respect to events, such as sudden obstacles or rapidly changing traffic signals. We believe that unpredictable future events and corresponding expert reactions can introduce reasoning disturbances, negatively affecting the convergence efficiency of planning models. At the same time, long-term decision information, such as maintaining a reference lane or avoiding stationary obstacles, is essential for guiding short-term decisions. Our preliminary experiments on shortening the planning horizon show a rise-and-fall trend in driving performance, supporting these hypotheses. Based on these insights, we present PlanScope, a sequential-decision-learning framework with novel techniques for separating short-term and long-term decisions in decision logs. To identify and extract each decision component, the Wavelet Transform on trajectory profiles is proposed. After that, to enhance the detail-generating ability of Neural Networks, extra Detail Decoders are proposed. Finally, to enable in-scope decision supervision across detail levels, Multi-Scope Supervision strategies are adopted during training. The proposed methods, especially the time-dependent normalization, outperform baseline models in closed-loop evaluations on the nuPlan dataset, offering a plug-and-play solution to enhance existing planning models.

The source code and associated videos are available at <https://github.com/Rex-sys-hk/PlanScope>.

I. INTRODUCTION

Imitation learning has played a pivotal role in advancing the progress of urban autonomous driving [1], [2]. In particular, learning from driving logs of experts is broadly adopted to supervise neural networks for the planning task. During the training process, distance error is commonly employed, which is to measure the discrepancy between the planned state sequence and the expert demonstrations, thereby optimizing parameters of the neural network [3]–[7]. Yet, when training learning-based planning systems, it is not absolutely reasonable to set the logged expert states as the target sequence, because future events are inherently uncertain, and potential disruptions such as unexpected obstacles or fluctuating traffic signals can significantly alter the trajectory planning.

This work was supported by the Guangzhou Education Bureau Project under Grant 2024312095. (*Corresponding author: Jun Ma.*)

Ren Xin, Hongji Liu, and Jun Ma are with the Division of Emerging Interdisciplinary Areas, The Hong Kong University of Science and Technology, Hong Kong SAR, China, and also with the Robotics and Autonomous Systems Thrust, The Hong Kong University of Science and Technology (Guangzhou), Guangzhou 511453, China (e-mail: rxin@connect.ust.hk; hliucq@connect.ust.hk; jun.ma@ust.hk).

Jie Cheng is with the Department of Electronic and Computer Engineering, The Hong Kong University of Science and Technology, Hong Kong SAR, China (e-mail: jchengai@connect.ust.hk).

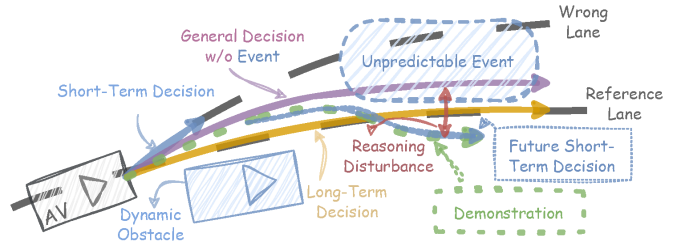


Fig. 1. In the scenario presented, the ego Autonomous Vehicle (AV) (black rectangle) is driving on a structured road with dynamic obstacles (blue rectangle). Its long-term decision (orange arrow) is characterized by adherence to the reference line (black long dash) for driving. Conversely, the short-term decision (blue arrow) involves evading the approaching dynamic object through the application of lateral velocity. Long-term and short-term decisions constitute the general decision (purple arrow) at the moment. However, the demonstrated trajectory (green dashed arrow), which incorporates future short-term decisions (blue dashed arrow) to avoid unpredictable events (blue dashed area), is counterintuitive in the current context and introduces unexpected reasoning noise (red double-headed arrow).

These unpredictable elements necessitate agile and nuanced adjustments to driving behavior. Some seemingly predictable decisions, such as behaviors in Game Theory models [8], [9] with multiple Nash Equilibria and switching traffic lights, are difficult to accurately predict. Meanwhile, a short-sighted planner is also not desirable, as the planner also needs to keep its long-term decision in consideration when choosing sudden maneuvers. Essentially, the state sequence of experts recorded in the log is a combination of short-term and long-term decisions under different scopes. A diagram of this concept is shown in Fig. 1. Due to the lack of observable information, long-term decisions are more susceptible to unpredictable events compared to short-term decisions. In learning targets like Average Distance Error (ADE), waypoints near the given current state only account for a small proportion of error compared to remote ones. This will result in a situation where unpredictable events occurring at the distant future affect current short-term decisions unexpectedly. This issue is evident during the training phase of the planning model, where it can lead to uneven convergence priorities or errant convergence over time. In summary, when training from expert demonstrations, trajectories inherently mix short-term reactive maneuvers and long-term directional decisions. Such entanglement often causes planning models to overfit to static future patterns and respond suboptimally to unexpected events. Therefore, considering the decision scope (DS) in the model training phase is crucial for making rational and efficient planning decisions. This work addresses this problem by introducing learning-based decision-scope-aware trajectory planning for urban autonomous driving.

Addressing the decoupling issue of information from vari-

ous decision scopes for imitation learning presents significant challenges. Traditional planning methods divide the problem into distinct layers: path planning, behavior planning, and motion planning. Specialized modules handle each of these layers. In contrast, imitation learning approaches often focus on learning future trajectories of a fixed length. This focus arises because nuanced adjustment components and long-term decision components are challenging to separate from log replay. One potential solution is to employ manual annotation for driving behavior reasoning. This method can help analyze both long- and short-term decisions, allowing the identification of behavior duration and start times. However, this approach entails a substantial workload and poses scalability challenges. Consequently, finding a cost-effective way to decouple decision scopes in the age of learning-based planning remains a complex issue under exploration.

To extract decision components from expert trajectories in an unsupervised manner, we propose using Wavelet Transform (WT) for temporal-frequency decomposition, where short-term decisions correspond to higher-frequency bands and long-term decisions to lower ones. After identifying these components, we develop Detail Decoding (DD) structures to enable Neural Networks (NNs) to generate detailed outputs. These NN-generated details are then supervised using Multi-Scope Supervision (MSS) techniques, including leveraging weighted loss and decomposed expert driving logs for supervision. Upon these designs, experimental validations of these strategies are conducted to ensure a comprehensive and practical exploration. Through our experiments, the most effective method is identified for enhancing model performance in closed-loop evaluations. Our contributions are fourfold:

- We propose PlanScope, a decision-scope-aware planning framework that explicitly models the relationship between temporal horizon and planning performance.
- We propose and validate the functionality of adopting WT to extract and analyze decision components in different frequency bands from expert demonstrated trajectories.
- We develop DD structures that are able to recursively refine trajectory velocity details across multiple temporal levels.
- We design novel MSS strategies based on wavelet decomposition and weighted loss to supervise learning at different motion frequencies and time horizons.

II. RELATED WORKS

A. Learning Strategies on Making Sequential Decisions

Sequential decision-making can be encapsulated with the framework of Partially Observable Markov Decision Processes (POMDPs) [10]. In this framework, the ego agent must make decisions based on environmental observations, anticipate subsequent states following its actions, and maximize the cumulative reward. Temporal difference (TD) together with Bellman Function formulates the basis of RL. In terms of RL for autonomous driving, it requires exponentially increasing search volume to find a feasible solution. This results in significant challenges when exploring optimized policies within high-dimensional state spaces, leading to substantial computational intensity. Consequently, this necessitates a high cost in terms

of real-world or simulation trials. Although modern learning strategies [11]–[13] significantly improve exploring efficiency and optimality, they still require millions of trials and are still impractical for real-world implementation for autonomous driving because of the safety issue.

Imitation Learning (IL) is an alternative approach that learns policies directly from expert demonstrations, thereby circumventing the need for explicit world models and reward functions [1], [2]. However, existing IL methods often overlook the temporal and causal relationships inherent in sequential decision-making processes. Whole-trajectory imitation typically treats all trajectory points equally, disregarding the varying significance of decisions made at different time scales within recognized driving patterns or history. This oversight can lead to suboptimal performance, particularly in complex scenarios where decisions at different time scales have varying levels of importance. Essentially, methodologies for solving these problems are under exploration. Data augmentation, reason labeling, and scaling up the dataset are commonly used to alleviate the problems of distribution shift [5]. Inductive bias can be introduced to alleviate these problems to some extent, like considering the reference lane as a strong prior [4], [14], or using an additional module to predict the traveling target first [15]–[17]. But a generalizable method for extracting in-scope decisions from expert demonstrations with less intensive labor remains underexplored.

B. Hierarchical Paradigm for Problem Simplification

In the context of traditional rule-based autonomous driving systems, in-time reaction and predictive decision are both required, making it challenging to determine the optimal policy sequence based on POMDP in real-time [18]. Hence, under traditional planning frameworks, hierarchical structure is typically employed to streamline computations [19], [20]. In the hierarchical structure, the planning problem is decomposed across various frequency bands, each with distinct hierarchical tendencies. For large-scale long-term decisions, one might opt for a lower resolution and focus on static objects by constructing maps [21], [22]. Conversely, within the smaller-scale areas identified by the large-scale search, the planner can leverage higher accuracy and decision correcting frequency to deal with dynamic objects control inaccuracies [23], [24].

The underlying mathematical principles can be traced to the Taylor expansion, which approximates complex polynomials with lower-order, linearized functions near a reference point [25]. In our work, we draw inspiration from this framework to develop a learning-based scope-aware planning model that effectively facilitates long-term stability and short-term flexibility.

C. Signal Time-Frequency Analysis

Expert driving logs contain various decision components, and extracting these components to supervise planning model outputs is a promising strategy for enhancing performance. Signal analysis has long been used to extract meaningful information from complex data. Analytical tools like the Fourier Transform (FT), Laplace Transform (LT), and Hilbert Transform (HT)

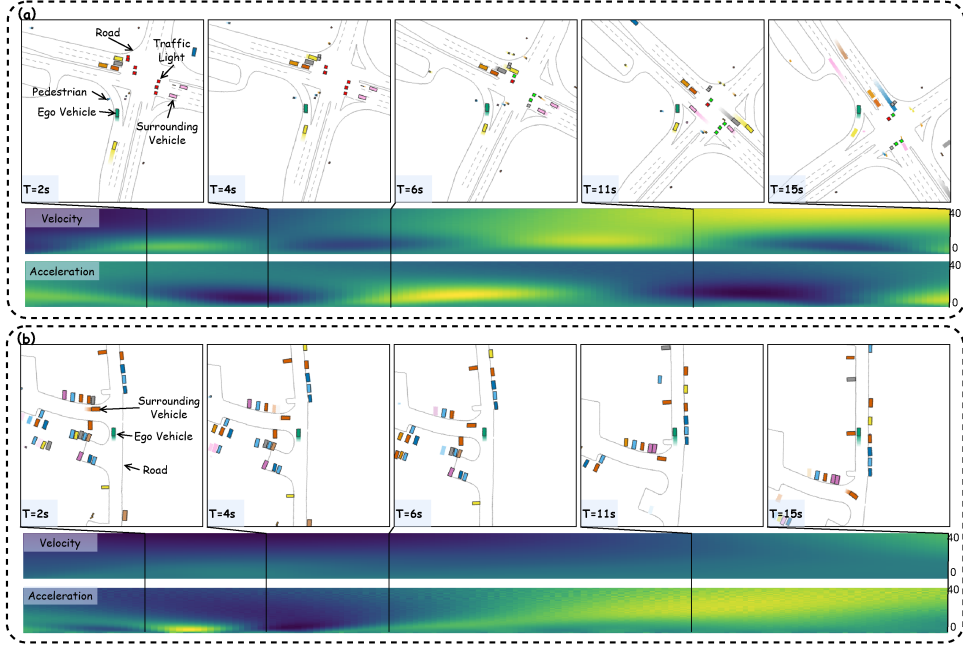


Fig. 2. Typical scenarios involving multi-scope decisions. (a) The long-term decision is a left turn. Between $T = 2$ s and $T = 4$ s, the vehicle stops to yield to pedestrians, then accelerates at $T = 6$ s to complete the turn. From $T = 6$ s and $T = 11$ s, it stops again upon observing the green light for cross traffic. (b) The ego vehicle first accelerates, then decelerates to secure the right of way. After observing another vehicle stop at $T = 4$ s, it gradually resumes acceleration. CWT of expert velocity and acceleration profiles follows below. In scenario (a), the area where the scale of wavelengths larger than 20 indicates a general speed increase as the vehicle transitions from a branch road to a main street. At smaller scales, two deceleration segments correspond to two reactive yielding maneuvers. In scenario (b), acceleration decomposition reveals an accelerate-then-decelerate decision around $T = 4$ s, and a gradual speed-up around scale 25 between time steps 8-15. The colorbar for coefficient amplitude is omitted since it is unnecessary for qualitative analysis.

are commonly employed for frequency-domain analysis [26]–[29]. For time–frequency signals, Short Time Fourier Transform (STFT) and WT are widely used to analyze non-stationary signals, with WT offering multi-resolution analysis that adapts to the signal characteristics, making it effective for capturing transient features [30], [31]. WT has been applied in autonomous driving, such as in [32] for categorizing car-following behaviors, preprocessing signal approximations, and identifying driving patterns through clustering. In [33], vehicle state records are analyzed using WT for driver identification, achieving nearly 100% accuracy with classifiers like XGBoost. In [34], wavelet-based decomposition of high-resolution maps improves path and motion planning. These applications demonstrate the effectiveness of WT in extracting features across diverse domains. Inspired by these works, we propose using WT to extract valuable information from expert trajectories for supervising decision-making across different time horizons.

III. METHODOLOGY

A. Scenario Analysis

In Fig. 2, we illustrate two typical cases involving multi-scope decisions to further elaborate on the proposed concept. Continuous Wavelet Transform (CWT) using the Gaussian basis function is applied to capture driving maneuvers for the two cases. We choose CWT over Discrete Wavelet Transform (DWT) to smoothly capture the changing patterns of coefficients across small to large scales. Because the Gaussian mother wavelet is a simple and widely adopted single-peak function, it can more effectively reflect the variance in trajectory profiles. From these two cases, we can clearly observe the additivity of self-driving maneuvers and unpredictability of certain traffic participants.

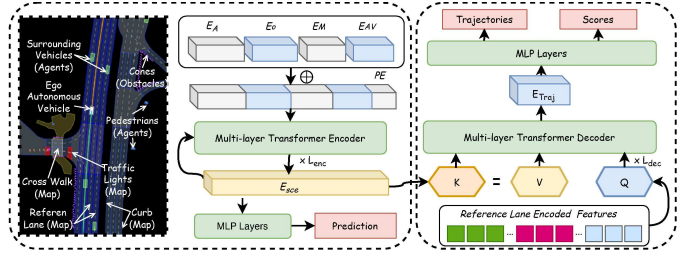


Fig. 3. The overall model framework initiates with the individual embedding of driving context elements, including the Dynamic Agents (A), Static Objects (O), Autonomous Vehicle (AV), together with High-Definition Map, Traffic Signs, and Signals (M), followed by their concatenation with positional embedding (PE) [35]. This concatenated context is subsequently processed through a Multi-layer Transformer encoder, iterated L_{enc} times. The scenario embedding serves as Key (K) and Value (V) of the transformer decoder and is decoded to formulate agent predictions, which serve to supervise the model’s understanding of the driving context comprehensively. The reference lane embedding and anchor-free variables are combined to form a Query (Q) for the scenario embedding.

By generating trajectories in a multi-scope paradigm, the model at each level should be simplified and converge with fewer samples. If we decompose a trajectory into three levels with three times the length, the n individual model cases should be simplified from $O(n \times 3n \times 9n)$ to $O(3n)$.

B. Problem Formulation & System Overview

Our research focuses on improving the trajectory quality generated by planning systems for urban autonomous driving, thereby contributing to driving efficiency and safety. At each time step, the autonomous vehicle is tasked with planning a future trajectory \mathcal{T} under various traffic-related contexts C_t . Each trajectory point has six channels: $[p_x, p_y, \cos \eta, \sin \eta, v_x, v_y]$. To ensure continuity in angle representation, the heading orien-

tation is encoded as $(\sin \eta, \cos \eta)$, which avoids the periodic discontinuity at $\pm\pi$. Driving contexts encompass dynamic agents (A), static objects (O), and Vectorized High-Definition Map (M) information. Generated outputs at time step t , denoted as G_t , include motion predictions \mathcal{P} of other agents, a multi-modal trajectory score \mathcal{S} , and detailed trajectory information \mathcal{D} at different levels of detail. A basic formulation of this framework can be represented as follows:

$$C_t = \{A_t, A_{t-1}, \dots, O_t, M_t, AV_t\}, G_t = \{\mathcal{T}, \mathcal{P}, \mathcal{S}, \mathcal{D}\},$$

$$G_t = f(C_t|\theta), \text{ w.r.t. } \theta = \arg \min \mathcal{L}(G_t, \hat{G}_t),$$

where f denotes the Neural Network (NN) model, θ is the model parameter, \mathcal{L} is the loss function, and \hat{G}_t is the ground truth of G_t from logged context.

Driving contexts are encoded as E_A, E_O, E_M, E_{AV} by Feature Pyramid Network (FPN) [36], Multi Layer Perceptron (MLP), PointNet [37] based vector encoder and State Dropout Encoder (SDE) [38], respectively. As shown in Fig. 3, the encoder is structured as a multi-layer transformer, which is widely adopted in [4], [5]. The decoder is carefully designed as described in III-E, generating trajectories that serve as references for a Linear Quadratic Regulator (LQR). During training, common auxiliary losses are integrated to supervise trajectory generation. The training losses include prediction loss \mathcal{L}_{pre} , and collision loss \mathcal{L}_{col} , which can be expressed by

$$\mathcal{L}_{\text{pre}} = \text{L1}_{\text{smooth}}(\mathcal{P}, \hat{\mathcal{P}}), \mathcal{L}_{\text{col}} = \frac{1}{T_f} \sum_{t=1}^{T_f} \sum_{i=1}^{N_c} \max(0, R_c + \epsilon - d_i^t),$$

where \mathcal{L}_{pre} measures trajectory discrepancy between generated and that from the dataset, \mathcal{L}_{col} computes the invasion distance by N_c circle-based vehicle outlines over T_f future steps, R_c denotes the summed radius of ego and agent circles, ϵ is the tolerance, and d_i^t represents the center distance at time t . Inspired by [14], [39], [40], the decoder query combines reference lane encodings with anchor-free learnable variables, forming the initial query Q_0 for multi-layer transformer decoding and subsequent residual updates of Q . During training, the final query Q_N is then forwarded to the trajectory MLP decoder and scoring MLP decoder, yielding the multi-modal trajectory and the score by

$$\mathcal{T} = \text{MLP}(Q_N), \pi = \text{MLP}(Q_N),$$

$$\mathcal{L}_{\text{cls}} = \text{CrossEntropy}(\pi, \hat{\pi}),$$

where $\hat{\pi}$ is a one-hot vector indicating the trajectory closest to the logged trajectory. Finally, the overall training loss is

$$\mathcal{L} = \mathcal{L}_{\text{reg}} + \mathcal{L}_{\text{cls}} + \mathcal{L}_{\text{pre}} + \mathcal{L}_{\text{col}} + \mathcal{L}_{\text{ds}},$$

where \mathcal{L}_{reg} is the weighted regression loss and \mathcal{L}_{ds} is the loss to supervise learning within decision scope. More details on weights design, acquisition of supervision signals, and the decoding of detailed information are elaborated in Section III-C, Section III-D, and Section III-E.2, respectively.

C. Weighted Loss

To emphasize certain parts in demonstrated trajectories, it is an alternative to consider the precision of waypoints at each time step as separate tasks. Using time-dependent weight along the

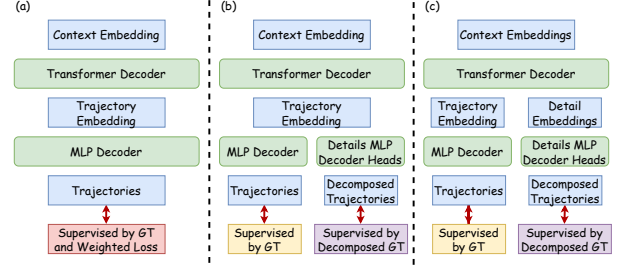


Fig. 4. Multi-scope trajectory supervision is achieved in three forms: (a) time-weighted loss on the baseline; (b) decoding final embedding as both full and decomposed trajectories; (c) iteratively decoding multi-scope detail embeddings as corresponding trajectory details.

decision sequence is a promising way to balance convergence pace across tasks, as shown in Fig. 4(a). The weighted regression loss can be calculated by

$$\mathcal{L}_{\text{reg}t} = \text{L1}_{\text{smooth}}(\mathcal{T}_t, \hat{\mathcal{T}}_t),$$

$$\mathcal{L}_{\text{reg}} = \frac{1}{T} \sum_{t=0}^T \mathcal{L}_{\text{reg}t} \times w_t,$$

where w_t can be designated by the following methods:

1) *Time Truncation*: Only the loss of the first T time steps is considered. In implementation, the executed trajectory is shortened to remove the influence of uncontrolled waypoints

$$w_t = \begin{cases} 1, & t < T, \\ 0, & t \geq T. \end{cases}$$

2) *Decreasing Certainty*: Those unpredictable disturbances might affect convergence capability on more important features and information for immediate decision. To describe this problem, we assume the sequential decision process conforms to the Gaussian Process (GP). The trajectory points $\mathbf{y}(t)$ can be modeled as outputs of a GP, with the mean and covariance determined by a kernel function $k(t_i, t_j)$, which can be a Radial Basis Function (RBF). Assuming the current state is an observable point, the variance of the predicted point at t can be easily derived by

$$\sigma_t^2 = \sigma_f^2 \left[1 - \exp\left(-\frac{(t-t_0)^2}{l^2}\right) \right],$$

where σ_f^2 is the function uncertainty, which can also be considered as the maximum uncertainty, l is the time length scaler, t_0 is the observable current time, which is set to 0 in the calculation. We define the uncertainty compensation as the deviation of maximum uncertainty:

$$\text{Compensation}(t) = \sigma_f^2 - \sigma_t^2.$$

Then, the calculation of weights to regularize uncertainty at each time point can be simplified as

$$w_t = \frac{1}{Z} \exp\left(-\left(\frac{t-t_0}{l}\right)^p\right),$$

where Z is the average weight. p is the order of the time difference measurement, which is 2 for RBF.

3) *Time Dependent Normalization*: To convert the value of data to the same order of magnitude or limit it to a certain range, we borrow the idea of Batch Normalization (BN). By

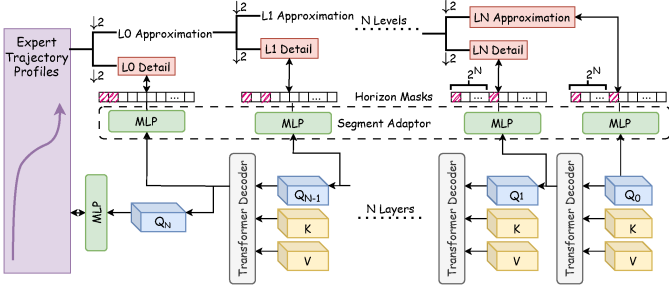


Fig. 5. The iterative detail decoder uses reference lane encoding as the initial query for multi-layer attention. At each iteration, extracted detail coefficients are combined with the previous query to refine further detail extraction. The initial query provides an approximation, and both it and subsequent generated details are processed via an MLP. The resulting detail embeddings are then mapped and compared against corresponding components at each level, with horizon masks configurable per level.

time-dependent normalization, the average error e_t of each time step across the mini-batch can be dynamically calculated by

$$BN(e_t) = \frac{e_t - \mu_{B:t}^{e_t}}{\sigma_{B:t}} = \frac{e_t}{\mu_{B:t}^{|e_t|}}, \text{ when } \mu_{B:t}^{e_t} = 0.$$

So, the distance error at each timestep e_t can be normalized by multiplying by weights

$$w_t = \left(\frac{1}{B} \sum_{b=1}^B \mathcal{L}_{regb:t} \right)^{-1},$$

where b is the index of the data item in the mini-batch and B is the batch size.

D. Expert Driving Logs Decomposition

In order to obtain decision components in the trajectory logs and selectively study them, we decompose them through mathematical analysis tools. By treating trajectory profiles as temporal signals, we use the Haar wavelet as the basis function for DWT. DWT is preferred over CWT due to its higher computational efficiency, facilitated by discrete downsampling at each wavelet scale, which is crucial for batch processing. The Haar wavelet is selected for its compact support, strong response to discontinuities, and identity property, making it well-suited to capture abrupt driving maneuvers like braking or lane changes, while minimizing bias. In the trajectory decomposition context, the trajectory approximation coefficient \mathcal{T}_A and the detail coefficient \mathcal{T}_D can be derived by performing the following transformation over the time horizon

$$\mathcal{T}_{A_t} = \sum_k \mathcal{T}[k] \phi(2t - k), \quad \mathcal{T}_{D_t} = \sum_k \mathcal{T}[k] \psi(2t - k),$$

where $\mathcal{T}[k]$ is the discrete trajectory profile, \mathcal{T}_{A_t} is the low-frequency approximation coefficient at time index t , \mathcal{T}_{D_t} is the high-frequency detail coefficient at time index t , k can be considered as the convolution handler. For Haar wavelet decomposition, \mathcal{T}_{A_t} represents the sum of $\mathcal{T}[k]$ and $\mathcal{T}[k+1]$ while \mathcal{T}_{D_t} is the product similarities bwtween $[\mathcal{T}[k], \mathcal{T}[k+1]]$ and $[1, -1]$. This decomposition process is called DWT, which can be recursively applied to the approximation coefficient \mathcal{T}_A to achieve multi-level l decomposition. By

$$\left(\mathcal{T}_A^l, \mathcal{T}_D^l \right) = \text{DWT} \left(\mathcal{T}_A^{l-1} \right),$$

we decompose trajectory profiles into N levels. The profile in our experiments is selected to be the coordinate values of waypoints. The approximation obtained in the last level is nominated as the preliminary decision. With the extraction of a detail component in each level, the length of the data is reduced by half.

E. Detail Decoding

Since the decomposed trajectory profile has been obtained, the question arises as to how it can be effectively utilized to guide the supervision of the model training process.

1) *Multi-head Detail Decoder (MDD)*: As shown in Fig. 3 and 4 (b), the transformer decoder layer generates trajectory embedding. Benefits from the function-fitting ability of MLPs, each decoding head with an MLP is able to decode trajectory embedding to details of designated levels or the overall approximation without interference. This process can be expressed as

$$\tilde{\mathcal{T}}_A^N = \text{MLP}(Q_N), \quad \tilde{\mathcal{T}}_D^l = \text{MLP}_l(Q_N),$$

where the tilde means the trajectory detail and approximation is predicted by the model. This design aims to train MLPs as detail extractors across different levels, without introducing artificial intervention or associated bias.

2) *Iterative Detail Decoder (IDD)*: To facilitate the learning of detailed information, IDD is designed, which is capable of progressively generating details across multiple iterations as shown in Fig. 4 (c). The architecture of the IDD is depicted in Fig. 5. In the decoding process, the embedding of the reference lane serves as the query Q_0 , and scenarios encoding E_{sce} serves as the key and value for a series of self-attention operations. We hypothesize that the multi-layer transformer decoder serves as a trajectory refining process. This hypothesis is based on the observation that the layer normalization operation within each decoding layer reduces information capacity while enhancing accuracy. The embeddings extracted at each iteration are accumulated with the previous query, which is then utilized as the subsequent query. The process can be described as

$$Q_i = \text{TransformerDecoder}(Q_{i-1}, E_{sce}, E_{sce}).$$

In the decoding process, the transformed feature Q_i is generated during each iteration and recorded. Logged $\{Q_i\}$ is adapted by level-wise MLP decoders, i.e.,

$$\tilde{\mathcal{T}}_A^N = \text{MLP}_A(Q_0), \quad \tilde{\mathcal{T}}_D^l = \text{MLP}_l(Q_l).$$

The length of $\tilde{\mathcal{T}}$ is the same as the planning steps. To make sure the decoded details are of the same length as the driving details, downsampling is performed on $\tilde{\mathcal{T}}$ by

$$\mathcal{T}_A^N = \tilde{\mathcal{T}}_A^N \downarrow 2^N, \quad \mathcal{T}_D^l = \tilde{\mathcal{T}}_D^l \downarrow 2^{l+1}.$$

These details are compared with the corresponding components of expert trajectories at multiple levels. To get decision details in a proper scope, only a limited time horizon H_l of \mathcal{T}_D^l at level l is within the decision scope, supervising model training by

$$\mathcal{L}_{ds} = \frac{1}{N+1} \left(\sum_{l=0}^N \left(\|\mathcal{T}_D^l[:H_l] - \hat{\mathcal{T}}_D^l[:H_l]\|_2 \right) + \|\mathcal{T}_A^N - \hat{\mathcal{T}}_A^N\|_2 \right).$$

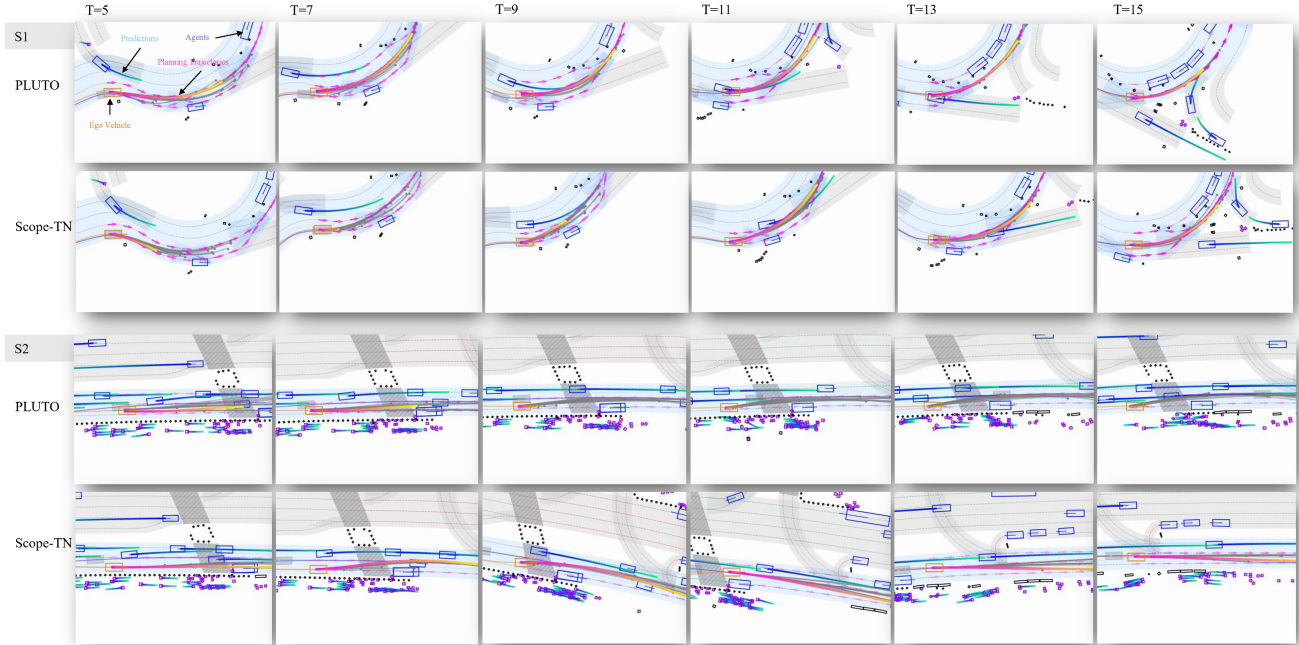


Fig. 6. The qualitative comparison is conducted between the standard PLUTO and PlanScope (Scope) with time-dependent normalization (TN), whose quantitative results are listed in Table II, fourth and third row from the bottom, respectively. In scenario **S1**, **PLUTO** fails to make a timely response to the impending collision in the short term, but chooses to continue along the long-term decision. In contrast, **Scope** makes a timely yielding maneuver. In scenario **S2**, **PLUTO** adopts a conservative decision due to the high uncertainty of the future trajectory caused by interaction with the rear vehicle in a long time horizon. In contrast, **Scope** adopts a human-like lane change decision.

TABLE I

PRELIMINARY ABLATION STUDIES ON DECODING AND SUPERVISION STRATEGIES

Detail Gen.		Supervision		Remarks	CLS-NR
Iterative	Detail Heads	Horizon	DWT		
-	-	80	-	PLUTO, m6	83.28%
-	-	10	-	Truncation	80.12%
-	-	20	-	Truncation	87.92%
-	-	40	-	Truncation	85.22%
-	-	-	-	Time decay	88.36%
-	-	-	-	Time norm	87.97%
-	✓	10	✓	Position	82.26%
✓	-	10	✓	Position	84.71%
-	✓	20	✓	Position	82.48%
✓	-	20	✓	Position	82.96%

IV. EXPERIMENTS

A. Implementation Details

Our training is conducted on the nuPlan dataset [41], which comprises a training set of 25,000 scenarios. We evaluate our model’s performance against baseline models within the nuPlan challenge framework. In addition, we conduct an ablation study to determine the significance of each component within our model. The training is performed on a server equipped with 8 NVIDIA L20 GPUs. We employ the Adam optimizer with a starting learning rate of 0.001, 3 warm-up epochs, and a batch size of 32 per GPU node over 25 training epochs. The PyTorch library is used to implement the model, with each training session lasting approximately 2 days.

Our evaluation is conducted on the **Val14** [42] subset of the nuPlan dataset, encompassing 1,090 validating scenarios. Each simulation entails a 15-second rollout at a frequency of 10 Hz. The evaluation score is derived using the official

evaluation script provided by the nuPlan challenge. Our primary comparison metric is the CLS-NR driving score, which is more challenging as other vehicles do not avoid collisions with the ego vehicle. Besides, the future step of our model is 80 while the history step is 21. Both our model and **PLUTO** [5] are set to generate six modal trajectories. In our experiments, the maximum horizons of decision scope across levels are controlled by setting **DS Horizon**, denoted h . Furthermore, we borrow the idea from [43] to facilitate the rapid implementation and execution of wavelet transformations in our experiments.

B. Preliminary Experiments

To identify truly effective strategies from the ones we explored, extensive comparative experiments are conducted. In these studies, all models are trained on 20% of the dataset for 35 epochs and evaluated on the **Random14** [42] test set, comprising 249 scenarios. The results are shown in Table I. The ablation study encompasses the following configurations: In the first experiment, we train the baseline model without additional peripheral losses, achieving a CLS-NR score of 83.28%. Rows 1-4 are designed to explore the existence of the PlanScope problem. In these experiments, we apply a Time Truncation Horizon of 10, 20, 40, and 80 time steps, respectively. The corresponding results are 80.12%, 87.92%, 85.22%, and 83.28%. The initially rising and subsequently falling score suggests that a planning horizon of 20 is relatively optimal. This corroborates our hypothesis that short-term decisions can improve planning performance. However, overly myopic decisions may introduce other issues, such as collisions due to the absence of predictive planning. Results from rows 5-6 demonstrate that weighting the regression loss enhances planning performance in closed-loop simulations. Specifically, the Decreasing Certainty weight

TABLE II
COMPARISON WITH BASELINE METHODS

Planner	Comfortness	Progress	w/o Collision	in Speed Limit	Drivable	TTC	CLS-NR	CLS-R
Log-Replay	99.27%	98.99%	98.76%	96.47%	98.07%	94.40%	93.68%	81.24%
IDM	79.31%	86.16%	90.92%	97.33%	94.04%	83.49%	79.31%	79.31%
RasterModel	81.64%	80.60%	86.97%	98.03%	85.04%	81.46%	66.92%	64.66%
UrbanDriver	100.00%	80.83%	94.13%	91.58%	90.83%	80.28%	67.72%	64.87%
GameFormer	93.39%	89.04%	94.32%	98.67	94.87%	86.77%	82.95%	83.88%
PLUTO-m6	95.14%	87.13%	94.45%	97.87%	98.90%	90.92%	85.81%	76.45%
PlanScope-Ih10-DWT	95.96%	86.04%	95.37%	98.20%	98.44%	91.74%	85.99%	75.81%
PlanScope-Mh20-DWT	97.89%	86.70%	93.72%	98.42%	98.81%	91.28%	85.80%	77.60%
PlanScope-Th20	99.27%	76.32%	95.50%	99.22%	99.36%	91.93%	83.86%	83.74%
PlanScope-timedecay	96.24%	86.34%	95.14%	98.24%	99.63%	91.56%	86.48%	75.22%
PlanScope-timenorm	98.26%	88.04%	96.28%	98.20%	99.45%	92.94%	88.41%	75.56%
PLUTO-m12-C	96.41%	93.28%	96.18%	98.13%	98.53%	93.28%	89.04%	80.01%
PlanScope-timenorm-m12-C	97.25%	89.54%	97.29%	98.04%	99.72%	93.85%	91.32%	80.96%
PLUTO-m12-C-H	91.93%	93.65%	98.30%	98.20%	99.72%	94.04%	93.21%	92.06%
PlanScope-timenorm-m12-C-H	93.85%	93.09%	98.35%	98.22%	99.82%	94.86%	93.59%	91.07%

The suffixes **m6/m12** denote that the trajectory mode number is set to 6 or 12, respectively. **Ih10** abbreviates IDD with a DS Horizon of 10, while **Mh10** refers to MDD with a DS Horizon of 10. **Th20** signifies the use of Time Truncation weights with a DS Horizon of 20. **C** denotes the application of contrastive learning. **H** represents a hybrid method combining learning and rule-based post-processing. **CLS-R** represents Reactive Closed Loop Simulation.

is denoted as *timedecay*, and Time-Dependent Normalization is denoted as *timenorm*. The demonstrated value of $p = 1$ and $l = e$ for *timedecay* achieves the best performance in our preliminary grid search. Comparisons in rows 7-10 indicate that IDD with DS Horizon 10 performs well in learning supervision signals obtained via DWT.

C. Comparison with Baselines

We conduct a comparative analysis of our method against several standard approaches; the comparative results are presented in Table II. **Log-Replay**, which entails a straightforward replay of expert trajectories, serves as a baseline reference. This demonstrates the capability of our simulator to assess the performance of planning algorithms accurately. **IDM** [44] employs the Intelligent Driver Model to maintain safe distances from other agents and adhere to the reference lane. **RasterModel**, introduced in [41], is a CNN-based planning model. **UrbanDriver** [45] is a vectorized planning model leveraging PointNet-based polyline encoders and transformer architecture. **PLUTO** [5], our primary baseline, achieves state-of-the-art performance in the nuPlan planning challenge in April 2024. To save computing resources, the multimodal trajectory mode number is set to m6 at first. By default, we have excluded the rule-based trajectory selector, thereby demonstrating that our new model enhances the performance of the neural planner. Besides, we also eliminate the contrastive learning module, which is empowered by rule-based positive and negative sample construction. These modules are removed to reduce artifacts that may introduce bias into the results. Our model, designated as **PlanScope**, is evaluated with various modules that perform well in preliminary experiments. Part of qualitative comparison is depicted and introduced in Fig. 6. The results in the table indicate that incorporating *timenorm* further improves the driving score in closed-loop simulations, achieving a total score of 93.59%. The capabilities of the post-processing module primarily constrain this improvement. Under a framework that relies solely on network-based output without post-processing, our closed-loop total score 91.32% increases

by 2.28% compared to the previous result. In experiments with mode number equals 6 and without contrastive learning, the model with *timenorm* also achieves the best CLS-NR score of 88.41%, which increases 2.6% compared to PLUTO-m6. We also observe that the score for *Time Truncation* is lower than the baseline, suggesting that a decision-making strategy focused solely on the short term may overlook critical long-term aspects. Additionally, methods based on detail generation and decomposition show slight improvement. More decomposition methods, decomposing profiles, wavelet forms, and related research on horizon adaptation might be required to enhance its performance further.

V. CONCLUSIONS

This paper identifies the reasoning gap of imitation learning for urban autonomous driving and formulates it as PlanScope, which has been overlooked in previous studies. The proposed WT-based trajectory decomposition and analysis technique, DD structures, and MSS strategies jointly enable trajectory refinement across decision scopes. These design eliminates unpredictable future events and their negative effects for training learning-based planners. Experiments on the nuPlan benchmark confirm that explicitly modeling motion scope yields consistent improvements in safety and efficiency metrics. Among these methods, the implementation of *timenorm* achieves a state-of-the-art 91.32% CLS-NR score in no-post-processing mode. In hybrid mode, it achieves a 93.59% CLS-NR score, which significantly surpasses the baseline. In addition, detail generation modes combined with our proposed decomposition methods show limited improvement. Their performance does not surpass that of *timenorm* and *timedecay*. Nonetheless, wavelet transformation provides a potential solution to this issue. We present these findings as a starting point for narrowing the exploration range for future research. In the future, we plan to conduct more thorough experiments to explore the mechanisms underlying this problem, including further investigation of combinations and loss balancing across levels of detail.

REFERENCES

- [1] M. Bansal, A. Krizhevsky, and A. Ogale, “Chauffeurnet: Learning to drive by imitating the best and synthesizing the worst,” in *Proceedings of the Conference on Robotics: Science and Systems*, 2019.
- [2] A. Hussein, M. M. Gaber, E. Elyan, and C. Jayne, “Imitation Learning: a survey of learning methods,” *ACM Computing Surveys*, vol. 50, no. 2, pp. 1–35, 2017.
- [3] S. Grigorescu, B. Trasnea, T. Cocias, and G. Macesanu, “A survey of deep learning techniques for autonomous driving,” *Journal of Field Robotics*, vol. 37, no. 3, pp. 362–386, 2020.
- [4] D. Dauner, M. Hallgarten, A. Geiger, and K. Chitta, “Parting with misconceptions about learning-based vehicle motion planning,” in *Proceedings of the Conference on Robot Learning*, 2023.
- [5] J. Cheng, Y. Chen, and Q. Chen, “PLUTO: push the limit of imitation learning-based planning for autonomous driving,” *arXiv preprint arXiv:2404.14327*, 2024.
- [6] H. Song, W. Ding, Y. Chen, S. Shen, M. Y. Wang, and Q. Chen, “PiP: planning-informed trajectory prediction for autonomous driving,” in *Proceedings of the European Conference on Computer Vision*. Springer, 2020, pp. 598–614.
- [7] T. Salzmann, B. Ivanovic, P. Chakravarty, and M. Pavone, “Trajectron++: Dynamically-feasible trajectory forecasting with heterogeneous data,” in *Proceedings of the European Conference on Computer Vision*. Springer, 2020, pp. 683–700.
- [8] X. Zhou, Z. Peng, Y. Xie, M. Liu, and J. Ma, “Game-theoretic driver modeling and decision-making for autonomous driving with temporal-spatial attention-based deep q-learning,” *Transactions on Intelligent Vehicles*, vol. 10, no. 7, pp. 4010–4025, 2025.
- [9] Z. Huang, H. Liu, and C. Lv, “GameFormer: game-theoretic modeling and learning of transformer-based interactive prediction and planning for autonomous driving,” in *Proceedings of the International Conference on Computer Vision*, 2023, pp. 3903–3913.
- [10] M. Hoerger and H. Kurniawati, “An on-line POMDP solver for continuous observation spaces,” in *Proceedings of the International Conference on Robotics and Automation*, 2021, pp. 7643–7649.
- [11] T. Haarnoja, A. Zhou, P. Abbeel, and S. Levine, “Soft Actor-Critic: off-policy maximum entropy deep reinforcement learning with a stochastic actor,” in *International Conference on Machine Learning*, 2018, pp. 1861–1870.
- [12] V. Mnih, A. P. Badia, M. Mirza, A. Graves, T. Lillicrap, T. Harley, D. Silver, and K. Kavukcuoglu, “Asynchronous methods for deep reinforcement learning,” in *Proceedings of the International Conference on Machine Learning*, 2016, pp. 1928–1937.
- [13] J. Schulman, S. Levine, P. Abbeel, M. Jordan, and P. Moritz, “Trust region policy optimization,” in *Proceedings of the International Conference on Machine Learning*, 2015, pp. 1889–1897.
- [14] J. Cheng, R. Xin, S. Wang, and M. Liu, “MPNP: Multi-Policy Neural Planner for Urban Driving,” in *Proceedings of the International Conference on Intelligent Robots and Systems*, 2022, pp. 10 549–10 554.
- [15] H. Zhao, J. Gao, T. Lan, C. Sun, B. Sapp, B. Varadarajan, Y. Shen, Y. Shen, Y. Chai, C. Schmid, et al., “TNT: target-driven trajectory prediction,” in *Proceedings of the Conference on Robot Learning*, 2021, pp. 895–904.
- [16] T. Gilles, S. Sabatini, D. Tsishkou, B. Stanciulescu, and F. Moutarde, “HOME: heatmap output for future motion estimation,” in *Proceedings of the International Intelligent Transportation Systems Conference*, 2021, pp. 500–507.
- [17] —, “GOHOME: graph-oriented heatmap output for future motion estimation,” in *Proceedings of the International Conference on Robotics and Automation*, 2022, pp. 9107–9114.
- [18] Y. Lee, P. Cai, and D. Hsu, “MAGIC: Learning Macro-Actions for Online POMDP Planning,” in *Proceedings of the Robotics: Science and Systems*, 2021.
- [19] W. Ding, L. Zhang, J. Chen, and S. Shen, “Epsilon: An efficient planning system for automated vehicles in highly interactive environments,” *Transactions on Robotics*, vol. 38, no. 2, pp. 1118–1138, 2021.
- [20] Y. Chen, J. Cheng, S. Wang, H. Liu, X. Mei, X. Yan, M. Tang, G. Sun, Y. Wen, J. Cai, et al., “Enhancing campus mobility: Achievements and challenges of the snow lion autonomous shuttle,” *Robotics & Automation Magazine*, 2024.
- [21] H. Liu, L. Zheng, X. Yan, Z. Xu, B. Xue, Y. Yu, and M. Liu, “Pgo-iplm: Enhance ipm accuracy with pose-guided optimization for low-cost high-definition angular marking map generation,” in *Proceedings of the Intelligent Vehicles Symposium*, 2024, pp. 1041–1046.
- [22] OpenStreetMap contributors, “Planet dump retrieved from <https://planet.osm.org>,” <https://www.openstreetmap.org>, 2017.
- [23] Y. Pan, Q. Lin, H. Shah, and J. M. Dolan, “Safe planning for self-driving via adaptive constrained ILQR,” in *Proceedings of the International Conference on Intelligent Robots and Systems*, 2020, pp. 2377–2383.
- [24] D. Lam, C. Manzie, and M. Good, “Model predictive contouring control,” in *Proceedings of the Conference on Decision and Control*, 2010, pp. 6137–6142.
- [25] B. Kouvaritakis and M. Cannon, “Model predictive control,” *Switzerland: Springer International Publishing*, vol. 38, no. 13-56, p. 7, 2016.
- [26] S. Bochner and K. Chandrasekharan, *Fourier transforms*. Princeton University Press, 1949, no. 19.
- [27] E. O. Brigham, *The fast Fourier transform and its applications*. Prentice-Hall, Inc., 1988.
- [28] J. L. Schiff, *The Laplace transform: theory and applications*. Springer Science & Business Media, 1999.
- [29] M. Feldman, “Hilbert transform in vibration analysis,” *Mechanical systems and signal processing*, vol. 25, no. 3, pp. 735–802, 2011.
- [30] L. Durak and O. Arikan, “Short-time fourier transform: two fundamental properties and an optimal implementation,” *Transactions on Signal Processing*, vol. 51, no. 5, pp. 1231–1242, 2003.
- [31] A. Graps, “An introduction to wavelets,” *Computational Science and Engineering*, vol. 2, no. 2, pp. 50–61, 1995.
- [32] Y. Zheng, S. He, R. Yi, F. Ding, B. Ran, P. Wang, and Y. Lin, “Categorizing car-following behaviors: wavelet-based time series clustering approach,” *Journal of Transportation Engineering, Part A: Systems*, vol. 146, no. 8, p. 04020072, 2020.
- [33] B. I. Kwak, M. L. Han, and H. K. Kim, “Driver identification based on wavelet transform using driving patterns,” *Transactions on Industrial Informatics*, vol. 17, no. 4, pp. 2400–2410, 2021.
- [34] R. V. Cowlagi and P. Tsiotras, “Multiresolution motion planning for autonomous agents via wavelet-based cell decompositions,” *Transactions on Systems, Man, and Cybernetics, Part B*, vol. 42, no. 5, pp. 1455–1469, 2012.
- [35] Z. Zhou, J. Wang, Y.-H. Li, and Y.-K. Huang, “Query-centric trajectory prediction,” in *Proceedings of the Conference on Computer Vision and Pattern Recognition*, 2023, pp. 17 863–17 873.
- [36] J. Cheng, Y. Chen, X. Mei, B. Yang, B. Li, and M. Liu, “Rethinking imitation-based planners for autonomous driving,” in *Proceedings of the International Conference on Robotics and Automation*, 2024, pp. 14 123–14 130.
- [37] C. R. Qi, H. Su, K. Mo, and L. J. Guibas, “PointNet: deep learning on point sets for 3d classification and segmentation,” in *Proceedings of the Conference on Computer Vision and Pattern Recognition*, 2017, pp. 652–660.
- [38] J. Cheng, X. Mei, and M. Liu, “Forecast-MAE: self-supervised pre-training for motion forecasting with masked autoencoders,” in *Proceedings of the International Conference on Computer Vision*, 2023, pp. 8679–8689.
- [39] N. Carion, F. Massa, G. Synnaeve, N. Usunier, A. Kirillov, and S. Zagoruyko, “End-to-end object detection with transformers,” in *Proceedings of the European Conference on Computer Vision*, 2020, pp. 213–229.
- [40] R. Xin, J. Cheng, S. Wang, and M. Liu, “Velocity Field: an informative traveling cost representation for trajectory planning,” in *Proceedings of the International Conference on Robotics and Biomimetics*, 2023, pp. 1–6.
- [41] H. Caesar, J. Kabzan, K. S. Tan, W. K. Fong, E. Wolff, A. Lang, L. Fletcher, O. Beijbom, and S. Omari, “nuPlan: a closed-loop ML-based planning benchmark for autonomous vehicles,” in *Proceedings of the Conference on Computer Vision and Pattern Recognition ADP3 Workshop*, 2021.
- [42] D. Dauner, M. Hallgarten, A. Geiger, and K. Chitta, “Parting with misconceptions about learning-based vehicle motion planning,” in *Proceedings of the Conference on Robot Learning*, 2023.
- [43] M. Wolter, F. Blanke, J. Garcke, and C. T. Hoyt, “ptwt - The PyTorch Wavelet Toolbox,” *Journal of Machine Learning Research*, vol. 25, no. 80, pp. 1–7, 2024.
- [44] S. Albeik, A. Bayen, M. T. Chiri, X. Gong, A. Hayat, N. Kardous, A. Keimer, S. T. McQuade, B. Piccoli, and Y. You, “Limitations and improvements of the intelligent driver model,” *Journal on Applied Dynamical Systems*, vol. 21, no. 3, pp. 1862–1892, 2022.
- [45] O. Scheel, L. Bergamini, M. Wolczyk, B. Osiński, and P. Ondruska, “Urban Driver: learning to drive from real-world demonstrations using policy gradients,” in *Proceedings of the Conference on Robot Learning*, 2022, pp. 718–728.